First principles calculations of vacancy–vacancy interactions in nickel: thermal expansion effects

El Hocine Megchiche, Claude Mijoule, Mohand Amarouche

First principles calculations of vacancy–vacancy interactions in nickel: thermal expansion effects

E H Megchiche[1], C Mijoule[2] and M Amarouche[1]

[1] Laboratoire de Physique et Chimie Quantique (LPCQ), Université Mouloud Mammeri, Tizi-ouzou, Algeria
[2] CIRIMAT UMR CNRS/INP/UPS, École Nationale d'Ingénieurs en Arts Chimiques et Technologiques (ENSIACET), 4 allée Emile Monso, B.P 44362, Toulouse cedex 4, France

E-mail: claude.mijoule@ensiacet.fr

Abstract

The energetic properties of the divacancy defect in fcc nickel are studied by *ab initio* calculations based on density functional theory. The formation and binding enthalpies of the divacancy in the first (1nn), second (2nn) and third (3nn) nearest-neighbor configurations are presented. Results show that the 1nn divacancy configuration is the most stable with a formation enthalpy H_{2v}^{f} of 2.71 eV and a small binding energy H_{2v}^{b} of 0.03 eV. In the 2nn configuration, the monovacancy–monovacancy interaction is repulsive, and it vanishes in the 3nn configuration. The migration process of the divacancy in its stable configuration is studied. We find that the divacancy migrates in the (111) plane by successive rotational steps of 60°. The corresponding migration enthalpy H_{2v}^{m} is predicted to be 0.59 eV, about half of that found for the monovacancy. For a better comparison of our results with high temperature experimental data, we have analyzed the effects of thermal expansion. Our results show that the inclusion of thermal expansion allows us to reproduce satisfactorily the experimental predictions.

1. Introduction

In metals, the configuration and concentration of various defects play important roles in many phenomena, such as solid phase transformation, dislocation sliding, impurity atom diffusion and crack formation [1]. Divacancies are considered to be formed by an attractive interaction between two monovacancies, and are thought to contribute at high temperature to the self-diffusion process in many fcc materials. Several experimental studies show an upward curvature in the Arrhenius plot of the atomic self-diffusion of face-centered cubic metals [2, 3]. Three causes may explain this behavior [2, 4, 5]: firstly an intrinsic temperature dependence of the enthalpy and entropy changes associated to the formation and migration of monovacancies [6–8], secondly a contribution of multiple monovacancy jumps [9], and finally the contribution of divacancies to the self-diffusion process [10]. Experimentally, the last reason is supported by the relatively high concentration of divacancies, C_{2v}, in nickel at the melting temperature, compared to that of monovacancies, C_{1v} (C_{2v}/C_{1v} of the order of 20%) [2, 11]. In a previous theoretical work [12] we showed that the activation energy, activation entropy and pre-exponential factor associated with the monovacancies are independent of the thermal expansion of the lattice, i.e. of the temperature, and therefore we concluded that the deviation from the Arrhenius plot of the self-diffusion coefficient in nickel in the range of high temperature is mainly due to the formation and diffusion of divacancies. Many experimental data on the formation H_{2v}^{f}, migration H_{2v}^{m}, binding H_{2v}^{b}, and activation Q_{2v} enthalpies of divacancies in nickel are available [11, 13, 14]. Unfortunately they are obtained from various experimental techniques and thus in a large range of temperatures. Starting from the experimental data on self-diffusion by Hoffman *et al* [15] and by taking into account the presence of divacancies as well as the temperature dependence of energies and entropies related to the formation and migration of monovacancies, Seeger and Schumacher [13] deduced that $H_{2v}^{f} = 2.42$ eV, $H_{2v}^{m} = 0.82$ eV, and $H_{2v}^{b} = 0.28$ eV. Maier *et al* [11] combined their self-diffusion measurements with those of

Table 1. Some experimental and theoretical values of the divacancy formation H^{f}_{2v}, migration H^{m}_{2v}, and binding H^{b}_{2v} enthalpies in nickel. All values are in eV.

	Experiment	Theoretical
H^{f}_{2v}	2.41, 2.59 [18][a], 2.92–3.10 [17][b], 2.42 [13][c], 2.46 [19][c],	2.13, 2.20 [30][d],2.66 [23][e], 2.93 [20][e], 2.99 [31][d], 2.734 [21][e], 2.86 [27][d], 2.50–2.75 [29][d], 2.98 [22][e], 2.73 [25][d], 2.68 [28][d]
H^{b}_{2v}	0.4 ± 0.2 [17][b], 0.51 [18][a], 0.33, 0.44 [19][c], 0.28 [13][c]	0.066 ± 0.014 [21][e], 0.12 [28][d], 0.268 [24][d], 0.21–0.34 [29][d], 0.40 [27][d], 0.09 [30][d], 0.44 [26][d], 0.23 [22][e], 0.04 [33][f] 0.004 [23][e], 0.25 [25][d] 0.067 [32][g], 0.19 [20][e], [21][d]
H^{m}_{2v}	0.99, 1.16 [18][a], 0.83, 1.12 [19][c], 0.82 ± 0.03 [13][c], 0.72 ± 0.07 [16][a]	0.19 [31][d], 0.66 [27][d], 0.33, 0.63 [30][d], 0.674 [22][e], 0.90 [25][d], 1.17 [26][d], 0.96, 0.47 [20][e], 0.47 [23][e]
Q_{2v}	3.58([18] and [19])[a,c], 4.15 ± 0.69 [2][c], 3.45 [14][c] 3.61–3.85 [11][c], 3.24 [13][c]	3.13 [23][e], 2.46, 2.83 [30][d], 3.40 [20][e], 3.63 [25][d], 3.52 [27][d], 3.53 [26][d], 3.65 [22][e]

[a] Electrical resistivity. [b] Positron annihilation. [c] Analysis of experimental data.
[d] Semi-empirical. [e] Molecular dynamics. [f] DFT–GGA. [g] DFT–LDA.

Bakker [14] in order to cover a large temperature region (542–1400 °C). They deduced a value of $Q_{2v} = 3.7$ eV. By an electrical resistivity measurement method, Mughrabi and Seeger [16] found $H^{m}_{2v} = 0.72 \pm 0.07$ eV, and $H^{b}_{2v} = 0.23$ eV. With positron annihilation techniques, Nanao *et al* [17] deduced a formation enthalpy of 3.10 ± 0.2 eV and a binding energy of 0.4 ± 0.2 eV. Finally, Neumann and Tölle [2] found an activation energy of 4.15 ± 0.69 eV by using self-diffusion data from Bakker [14] and Maier *et al* [11]. All experimental data are given in table 1.

To our knowledge, most theoretical determinations of the formation and migration enthalpies of a divacancy in nickel are obtained from calculations based on various semi-empirical methods such as molecular statics and dynamics calculations [20–23], the lattice statics model [24], or embedded atoms methods (EAM and MEAM) [25–31]. They lead to values ranging from 2.50 to 2.98 eV for H^{f}_{2v}, 0.19 to 1.17 eV for H^{m}_{2v}, and 0.004 to 0.44 eV for H^{b}_{2v}. Only two studies carried out in the framework of density functional theory (DFT) are found. The first one was performed by Klemradt *et al* [32] by using the DFT method in the local density approximation (LDA). The second one is that of Zhang and Lu [33] who used the projected augmentation wave (PAW) method in the generalized gradient approximation (GGA). The divacancy binding enthalpy was estimated to 0.067 eV in the first work and 0.04 eV in the second one. However, H^{f}_{2v} and H^{m}_{2v} were not reported in either work. All theoretical results are also given in table 1 showing that first principles calculations on the divacancy in fcc nickel are still lacking.

In this paper, we examine some energetic properties of the divacancy, i.e. its formation and binding enthalpies in three different configurations. The migration and activation energies of the divacancy in its stable configuration are also determined. Furthermore, in order to compare our results with experimental data, the effects of the dilatation and thus of the thermal expansion of the lattice are examined. This approach has been used successfully in a previous work [12] to calculate the bulk properties and monovacancy energies in nickel.

2. Method of calculation

The present calculations are carried out within the DFT formalism and the pseudo-potential approximation. They are performed by means of the Vienna *ab initio* simulation program (VASP) developed at the Institut für Materialphysik of the Universität Wien [34, 35]. The spin-polarized self-consistent Kohn–Sham equations are solved within the projected-augmented wave (PAW) method [36, 37]. This leads to a powerful efficiency concerning the computation time. The Perdew–Wang 91 functional (PW91) [38] is used to describe the exchange–correlation effects. It has been shown that this functional describes efficiently various structural, elastic, and magnetic properties of the bulk nickel within a relative deviation less than 4% [12]. Concerning the computational parameters, the plane-wave energy cut-off is fixed to 14.7 Ryd (400 eV) for all calculations independently of the size of the unit cell. On the other side, $4 \times 4 \times 4$ and $6 \times 6 \times 6$ Monkhorst–Pack [39] meshes are used to sample the Brillouin zone in the reciprocal space, depending on the size of the studied unit cell. To determine the formation and migration enthalpies of the divacancy, two sizes of fcc primitive cells were tested i.e. 32 and 108 lattice sites per unit cell, in order to minimize the nearest-neighbor vacancy interactions. We consider that the size dependence has converged when both H^{f}_{2v} and H^{m}_{2v} do not vary by more than 0.01 eV. In each case we take into account the lattice relaxation for both formation and migration enthalpy calculations. The relaxation is introduced by using a conjugate-gradient algorithm for the formation and migration enthalpies. All ions were allowed to relax in the first case. In the second case, all the ions were allowed to relax except for the migrating nickel atom which was restrained to remain on the (111) symmetry axis where the saddle point is located. The thermal expansion contribution to H^{f}_{2v}, H^{m}_{2v} and thus to Q_{2v} is estimated by studying their dependence with respect to the lattice parameter a. H^{f}_{2v}, H^{m}_{2v} and Q_{2v} were calculated for six values of the lattice parameter a. At constant pressure P, the vacancy formation enthalpy can be approximated well by the formation energy owing to the supercell used in the calculations. The formation enthalpy of the divacancy is given by

$$H^{f}_{2v} = E^{tot}_{2v}(N-2) - \frac{N-2}{N} E^{tot}(N) \qquad (1)$$

where $E^{tot}_{2v}(N-2)$ is the total energy of the supercell containing $N-2$ atoms and two monovacancies, and $E^{tot}(N)$ is the total energy of the supercell containing N atoms in the perfect bulk

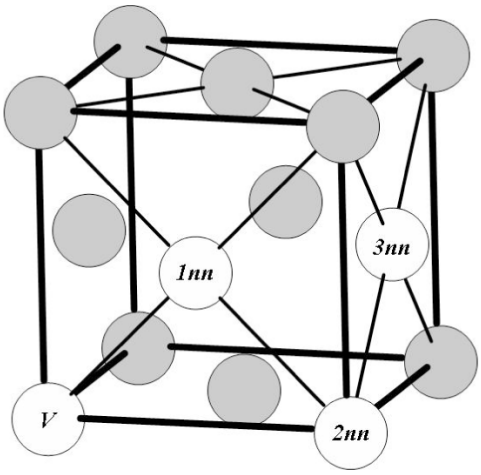

Figure 1. Configurations of divacancies in fcc structure. The open and full circles represent the vacancies and nickel atoms, respectively. Divacancies are formed between a monovacancy (V) and a first neighbor (1nn), second neighbor (2nn), or third neighbor (3nn) vacancy.

configuration. The binding energy of the divacancy E^{b}_{2v} is defined by

$$H^{b}_{2v} = 2H^{f}_{1v} - H^{f}_{2v} \quad (2)$$

where H^{f}_{1v} is the formation enthalpy of the monovacancy. With this convention, H^{b}_{2v} is positive when the vacancy–vacancy interaction is exothermic.

The migration enthalpy of the divacancy can be expressed as

$$H^{m}_{2v} = E^{sad}_{2v}(N-2) - E^{tot}_{2v}(N-2) \quad (3)$$

where $E^{sad}_{2v}(N-2)$ is the total energy of the supercell with $N-2$ nickel atoms, one of them being located at the saddle point. Finally, the activation energy Q_{2v} is given by

$$Q_{2v} = H^{f}_{2v} + H^{m}_{2v}. \quad (4)$$

3. Results and discussion

3.1. Energetics of the divacancy at 0 K

3.1.1. Formation and binding energies. The results obtained at 0 K (with an optimized lattice parameter of $a_0 = 3.52$ Å) for the formation and binding enthalpies of the first, second and third nearest-neighbor configurations (see figure 1) with 32- and 108-site supercells are listed in table 2. The most stable configuration corresponds to the first nearest neighbor (1nn) with a small binding energy $H^{b}_{2v} = 0.026$ eV. For the second 2nn and third 3nn nearest-neighbor configurations, the calculated binding energies are -0.1 eV (repulsive), and nearly 0 eV, respectively, showing that in this latter case there is no more interaction between vacancies. The repulsive character of the second nearest-neighbor conformation was previously obtained theoretically by Ackland *et al* [40]. The effect due to the lattice relaxation on the formation enthalpy is small, of the order of 0.12–0.15 eV in all cases; this is of the same order as that obtained by Simak and Andersson [41] for a 1nn divacancy in copper (0.18 eV). The lattice relaxation effects are

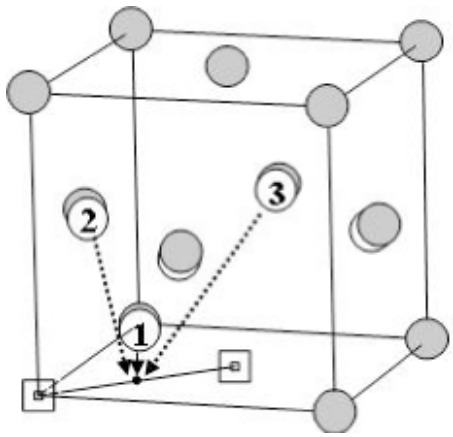

Figure 2. Schematic illustrating the relaxation in the neighborhood of a divacancy. Before (full circles) and after relaxation (open circles).

Table 2. Formation H^{f}_{2v} and binding H^{b}_{2v} energies (in eV) of the divacancy in the first neighbor (1nn), second neighbor (2nn) or third neighbor (3nn) for 32-site and 108-site supercells. Non-relaxed (Non-rel.) and relaxed (Rel.) values are presented.

		Formation enthalpy		Binding energy	
Size	Configuration	Non-rel.	Rel.	Non-rel.	Rel.
32	1nn	2.87	2.70	−0.01	−0.05
108	1nn	2.86	2.71	0.01	0.02
	2nn	2.96	2.83	−0.11	−0.09
	3nn	2.86	2.74	0.01	0.00
		Monovacancy [12]			
108		1.43	1.37		

principally due to the nearest-neighbor atoms surrounding the divacancy. The displacement of atoms around the divacancy in the 1nn configuration is schematically shown in figure 2. The relaxed atoms tend to contract towards the barycenter of the divacancy. This relaxation is of the order of 1.7%, 1.4%, and 0.9% of the optimized lattice parameter for the first, second and third neighbor conformations, respectively. The divacancy binding energies are not affected by the relaxation effects due to the compensation between those of the divacancy (0.15 eV) and the monovacancy (see equation (2) and table 2).

3.1.2. Migration and activation energies of a divacancy. In the fcc structure the divacancy migrates by successive rotation steps of 60° in the (111) plane. It was assumed in earlier works [23, 25] that the saddle point $S_{(111)}$ is located in the (111) plane at the barycenter of the equilateral triangle formed by the two monovacancies and the lattice site of the migrating atom, as shown in figure 3. Three of the nearest neighbors are located at a distance of $\frac{\sqrt{2}}{2}a$ and one at $\frac{1}{\sqrt{3}}a$. As pointed out by Neumann and Tuijn [42], this saddle point entails less symmetry than the saddle point S_{Ne} which has four equivalent first nearest neighbors located at a distance of $\frac{\sqrt{27}}{8}a$ (see figure 3). In that case, the saddle point does not belong to the (111) plane anymore. Our calculations agree with this last location (see table 3). Results for both $S_{(111)}$ and S_{Ne} positions

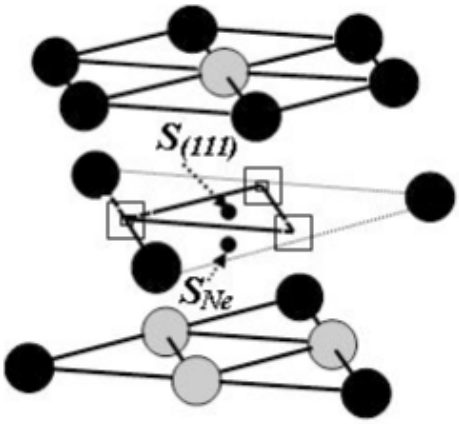

Figure 3. In plane ($S_{(111)}$) and out of plane (S_{Ne}) saddle points of the divacancy migration in the (111) plane. Nickel atoms are represented by full circles. Ni atoms, in gray, are the four nearest neighbors of the S_{Ne} migrating atom.

Table 3. Migration H^{m}_{2v} and activation Q_{2v} energies (in eV) of the divacancy in the first neighbor 1nn configuration for 32-site and 108-site supercells. Non-relaxed (Non-rel.) and relaxed (Rel.) values are presented.

		Migration enthalpy		Activation energy	
Saddle point	Size	Non-rel.	Rel.	Non-rel.	Rel.
$S_{(111)}$	32	1.10	0.89	3.97	3.59
	108	1.08	0.87	3.94	3.58
S_{Ne}	32	0.83	0.58	3.70	3.28
	108	0.81	0.59	3.67	3.30
			Monovacancy [12]		
	108	1.57	1.28	2.99	2.65

are given in table 3, showing that S_{Ne} corresponds to the true transition state. For the two supercell sizes, we obtained after relaxation migration enthalpies of 0.58 eV and 0.59 eV, respectively. The contribution of relaxation effects to the divacancy migration enthalpy (0.2 eV) is only slightly lower than that of the monovacancy migration enthalpy (0.3 eV) [12]. In fact, the nearest neighbors of the S_{Ne} saddle point are located at 2.29 Å while those of the monovacancy are situated at 2.16 Å, involving a larger repulsive interaction between the migrating atom and its nearest neighbors.

3.2. Thermal expansion effects

It has been shown in earlier works [12, 43] that the theoretical description of the formation energy of a monovacancy depends strongly on the approximation used for the exchange–correlation energy. One possibility to choose between these various approaches is to compare their ability to describe some well known properties of the bulk nickel. We summarize in table 4 some theoretical determinations of the lattice parameter, bulk modulus and cohesion energy for Ni, together with the corresponding formation energy of a monovacancy. Some of the data have been obtained by Delczeg *et al* who used an exact muffin-tin orbitals method [43]. The PAW–LSDA and PAW–GGA density functional approximation results are

Table 4. Equilibrium lattice parameter a_0, bulk modulus B, cohesion energy E_{coh} and monovacancy formation energy H^{v}_{f} for nine exchange–correlation approximations.

Method	a_0	B	E_{coh}	E^{f}_{1v}
PBE[a]	—	198	—	1.46
PBE[b]	6.66	—	4.67	1.40
LDA[a]	—	243	—	1.67
PBEsol[a]	—	223	—	1.67
AMO5[a]	—	222	—	1.75
LAG[a]	—	214	—	1.49
PAW–LSDA[c]	6.47	281	5.92	1.72
PAW–GGA[c]	6.66	195	4.64	1.43
US–GGA[b]	6.76	—	4.96	1.38
US–LDA[b]	5.90	—	6.10	1.71
Exp.	6.65	179–186	4.44	1.79 ± 0.05

[a] Reference [43]. [b] This work. [c] Reference [12].

from [12]. Finally, we have added results (US–LDA and US–GGA) obtained with the ultra-soft potential of Troullier and Martins [44] at the LDA and GGA levels. The results summarized in table 4 show that the best descriptions of bulk properties are obtained with PAW–GGA and PBE density functional approximations. The US–GGA gives slightly less accurate results. The corresponding calculated monovacancy formation energies lead nearly to the same result (of the order of 1.40–1.45 eV) far away from the recommended experimental data (1.79 eV). As the latter have been obtained at high temperature near the melting point, we have attributed the discrepancy between theory and experiment to thermal expansion effects.

Experimentally, the contribution of divacancies to the self-diffusion process in nickel is observed at temperatures near the melting point [2, 10, 11, 45]. Indeed, at high temperature, the contribution of divacancies to the diffusion process is significant, due to an increase of their concentration by an increase of the vacancy–vacancy binding energy and to their small migration enthalpy (0.59 eV at 0 K) compared to the monovacancies (1.28 eV at 0 K) allowing a larger mobility.

By involving simultaneously monovacancies and divacancies, the diffusion coefficient is described by

$$D = D_{1v} + D_{2v} = D^{0}_{1v} \exp\left(-\frac{Q_{1v}}{k_B T}\right) + D^{0}_{2v} \exp\left(-\frac{Q_{2v}}{k_B T}\right). \tag{5}$$

Q_{1v} and Q_{2v} are defined in equation (4), D^{0}_{1v} and D^{0}_{2v} are the frequency factors, k_B is the Boltzmann constant and T is the temperature in kelvin. Generally, a temperature dependence of energies $Q_{1v}(T)$ and $Q_{2v}(T)$ and entropies must be taken into account. From equation (4), the contribution of H^{f}_{2v} leads to an increase of $Q_{2v}(T)$; indeed, an increase of the temperature induces an increase of the divacancy formation entropy S^{f}_{2v} and thus an increase of H^{f}_{2v}, as can be seen from the following thermodynamic equation:

$$(\partial H^{f}_{2v}/\partial T)_p = T(\partial S^{f}_{2v}/\partial T)_p. \tag{6}$$

On the other hand, the divacancy migration enthalpy H^{m}_{2v} decreases with the lattice thermal expansion, due to a weakening of the nickel–nickel repulsion at the transition

Table 5. Thermal expansion effects on the divacancy formation, migration and activation energies (in eV). Results obtained with a 108-site unit cell size.

$\Delta a/a_0$ (%)	T (K)	H^{f}_{2v}	H^{m}_{2v}	Q_{2v}	H^{b}_{2v}
0	0	2.71	0.59	3.30	0.02
0.114	293	2.74	0.58	3.32	0.03
2.37	1600	3.25	0.52	3.77	0.07
2.67	1728	3.30	0.51	3.81	0.08
Exp.		3.10 ± 0.20[a]	0.72 ± 0.07[b]	4.15 ± 0.69[c]	0.23[b]

[a] Reference [17]. [b] Reference [16]. [c] Reference [2].

state. One way to introduce the electronic contribution to the temperature dependence is to consider that, as done in the ground electronic state, the electrons are moving in an effective potential created by the ions of the lattice located in a mean position corresponding to the lattice parameter at a given temperature. This is the well known Born–Oppenheimer approximation used in the ground state, where the vibration contribution is neglected. We can thus introduce temperature by using the thermal expansion data introduced by Suh *et al* [46] and collected by Lu *et al* [47] to determinate the coefficient of thermal expansion of nickel as a function of the temperature. This method has been used successfully to study the effect of thermal expansion on the energetic properties of a monovacancy in nickel [12] or on the atomic oxygen diffusion in nickel [48]. H^{f}_{2v}, H^{m}_{2v}, H^{b}_{2v}, and Q_{2v} have been calculated for several values of the relative linear expansion $\delta a/a_0$; results as well as their interpolations are represented in figure 4. The interpolated curves show that the formation enthalpy H^{f}_{2v} is increasing with $\delta a/a_0$, while the migration enthalpy H^{m}_{2v} is decreasing, as explained above. This leads finally to an increase of the self-diffusion energy. From our interpolated curves, we determined the various energies for $\delta a/a_0$ values associated to specific temperatures: absolute temperature (0 K), room temperature (293 K), average temperature for which the curvature of the Arrhenius plot has been observed (1600 K), and melting point temperature (1728 K). The results are summarized in table 5. They show that Q_{2v} depends significantly on the thermal expansion, contrary to Q_{1v} [12]. This is also true experimentally. In fact, The divacancy contribution in nickel is markedly smaller than in other metals and thus the error limits of vacancy parameters become considerable [2], the uncertainty on Q_{2v} reaching ± 0.69 eV. Nevertheless, only our upper values of Q_{2v} corresponding to larger thermal expansions belong to the experimental gap.

4. Conclusion

We briefly summarize our results. Vacancy–vacancy interaction in nickel is very weak when a divacancy is formed; it may even be slightly repulsive in the second nearest-neighbor configuration. The migration energy of the divacancy is nearly two times smaller than for the monovacancy allowing a much larger mobility. Though the displacement during diffusion arises by steps belonging to a (111) plane, transition states correspond to an out of plane saddle point. The introduction of

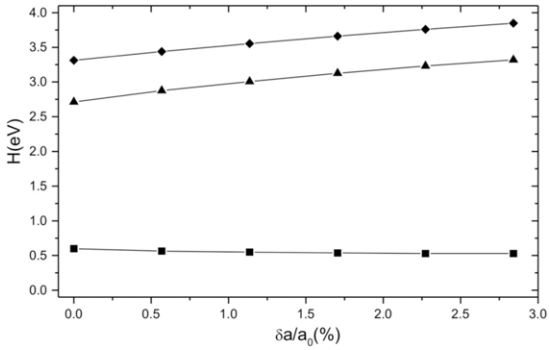

Figure 4. Relative linear expansion ($\delta a/a_0$) dependence of formation H^{f}_{2v} (▲), migration H^{m}_{2v} (■) and Q_{2v} (♦) enthalpies.

the electronic contribution to the dilatation of the lattice, i.e. to the thermal expansion, allows us to obtain formation and self-diffusion energy values in better agreement with experimental results. This is also the case for the determination of the vacancy–vacancy binding energy.

Acknowledgments

Computer resources for this work were provided by CALMIP (Toulouse, France) and the computer center GRID'5000 Nation-Wide Grid Experimental platform funded by the French Ministry of Research through the ACI GRID Program.

References

[1] Pérusin S, Viguier B, Monceau D, Ressier L and Andrieu E 2004 *Acta Mater.* **52** 5375
[2] Neumann G and Tölle V 1986 *Phil. Mag.* A **54** 619
[3] Siegel R W 1980 *Ann. Rev. Mater. Sci.* **10** 393
[4] Mehrer H 1978 *J. Nucl. Mater.* **69–70** 38
[5] Peterson N L 1978 *J. Nucl. Mater.* **69–70** 3
[6] Gilder H M and Lazarus D 1975 *Phys. Rev.* B **11** 4916
[7] Seeger A and Mehrer H 1970 *Vacancies and Interstitial in Metals* ed A Seeger, D Schumacher, W Schilling and J M Diehel (Amsterdam: North-Holland) p 1
[8] Mundy J N 1987 *Phys. Status Solidi* b **144** 233
[9] Da Fano A and Jacucci G 1977 *Phys. Rev. Lett.* **39** 950
[10] Peterson N L 1978 *Commun. Solid State Phys.* **8** 107
[11] Maier K, Mehrer H, Lessmann E and Schüle W 1976 *Phys. Status Solidi* b **78** 689
[12] Megchiche E H, Pérusin S, Barthelat J C and Mijoule C 2006 *Phys. Rev.* B **74** 064111
[13] Seeger A and Schumacher D 1967 *Mater. Sci. Eng.* **2** 31
[14] Bakker H 1968 *Phys. Status Solidi* **28** 569
[15] Hofman R E, Pikus R W and Schumacher D 1956 *Trans. AIME* **206** 483
[16] Mughrabi H and Seeger A 1967 *Phys. Status Solidi* b **19** 251
[17] Nanao S, Kuribayashi K, Tanigawa S and Doyama M 1977 *J. Phys. F: Met. Phys.* **7** 1403
[18] Schüle W and Scholz R 1982 *Point Defects and Defect Interactions in Metals* ed J Takamura, M Doyama and M Kiritani (Tokyo: University of Tokyo Press) p 257
[19] Schüle W and Scholz R 1979 *Phys. Status Solidi* b **93** K119
[20] García Ortega M, Ramos de Debiaggi S B and Monti A M 2002 *Phys. Status Solidi* b **234** 506
[21] Vasilyev A A, Strotinkin V V and Melker A I 1985 *Phys. Status Solidi* b **131** 537
[22] Shimomura Y 1997 *Mater. Chem. Phys.* **50** 139

[23] Lam N Q and Dagens L 1986 *J. Phys. F: Met. Phys.* **16** 1373
[24] Kornblit L 1983 *Phys. Status Solidi* b **115** 485
[25] Johnson R A 1966 *Phys. Rev.* **152** 629
[26] Baskes M I and Melius C F 1979 *Phys. Rev.* B **20** 3197
[27] Foiles S M, Baskes M I and Daw M S 1986 *Phys. Rev.* B **33** 7983
[28] Daw M S 1989 *Phys. Rev.* B **39** 7441
[29] Baskes M I 1997 *Mater. Chem. Phys.* **50** 152
[30] Munro L J and Wales D J 1997 *Faraday Discuss.* **106** 409
[31] Nemirovich-Danchenko L Y, Lipnitskiĭ A G and Kul'kova S E 2007 *Phys. Solid State* **49** 1079
[32] Klemradt U, Drittler B, Hoshino T, Zeller R, Dederichs P H and Stenanou N 1991 *Phys. Rev.* B **43** 9487
[33] Zhang X and Lu G 2008 *Phys. Rev.* B **77** 174102
[34] Kresse G and Hafner J 1993 *Phys. Rev.* B **47** 558
[35] Kresse G and Furthmuller J 1996 *Phys. Rev.* B **54** 11169
[36] Blochl P E 1994 *Phys. Rev.* B **50** 17953
[37] Kresse G and Joubert D 1999 *Phys. Rev.* B **59** 1758
[38] Perdew J P and Wang Y 1992 *Phys. Rev.* B **46** 12947
[39] Monkhorst H J and Pack J D 1976 *Phys. Rev.* B **13** 5188
[40] Ackland G J, Tichy G, Vitek V and Finnis M W 1987 *Phil. Mag.* A **56** 735
[41] Andersson D A and Simak S I 2004 *Phys. Rev.* B **70** 115108
[42] Neumann G and Tuijn C 2007 *Physica* B **396** 41
[43] Delczeg L, Delczeg-Czirjak E K, Johansson B and Vitos L 2009 *Phys. Rev.* B **80** 205121
[44] Troullier N and Martins J L 1991 *Phys. Rev.* B **43** 1993
[45] Kraftmakher Y 1998 *Phys. Rep.* **299** 79
[46] Suh I-K, Ohta H and Waseda Y 1988 *J. Mater. Sci.* **23** 757
[47] Lu X G, Selleby M and Sundman B 2005 *CALPHAD, Comput. Coupling Phase Diagr. Thermochem.* **29** 68
[48] Megchiche E H, Amarouche M and Mijoule C 2007 *J. Phys.: Condens. Matter* **19** 296201